Performance Optimization of EBG-Based Common Mode Filters for Signal Integrity Applications

Carlo Olivieri, Francesco de Paulis, Antonio Orlandi, and Slawomir Koziel

Abstract Electromagnetic bandgap structures have been shown to be effective in realizing simple and cheap common mode filters for differential interconnect applications in modern high-speed digital electronics. There are two major advantages offered by this technology. The first is that it relies on the standard planar layout methodology for filter design, applied to either a printed circuit board (PCB) or packaging materials and technology. The second advantage is easy analytical design procedure that requires full wave electromagnetic simulations only at a final stage for the filter geometry refinement to precisely meet given performance specifications. In this chapter, the latter aspect is enhanced by introducing an optimization stage that allows for automated adjustment of geometry parameters of the filter in order to improve its performance in terms of achieving the required central frequency, widening the bandwidth, and increasing the band-notch depth. The optimization approach proposed here combines fast response surface approximation modeling for initial design screening and local derivative-free design improvement using pattern search.

Keywords Optimization • Electromagnetic bandgap structures • Signal integrity • Filter • Common mode

MSC codes: 46N10, 65K10, 78A25 and 74F15

C. Olivieri • F. de Paulis • A. Orlandi (✉)
UAq EMC Laboratory, Department of Industrial and Information Engineering and Economics, University of L'Aquila, L'Aquila, Italy
e-mail: carlo.olivieri@univaq.it; francesco.depaulis@univaq.it; antonio.orlandi@univaq.it

S. Koziel
Engineering Optimization & Modeling Center, School of Science and Engineering, Reykjavik University, Menntavegur 1, 101 Reykjavik, Iceland
e-mail: koziel@ru.is

S. Koziel et al. (eds.), *Simulation-Driven Modeling and Optimization*,
Springer Proceedings in Mathematics & Statistics 153,
DOI 10.1007/978-3-319-27517-8_5

1 Introduction

Electromagnetic bandgap (EBG) structures are a sub-class of frequency selective surfaces. Introduced in 1999 [1] for applications in the field of antenna design and for minimization of the coupling between antennas [2–6], their usage has been extended to printed circuit boards (PCBs), mainly in the area of power integrity (PI) [7–16]. High-speed switches in digital systems generate well-known simultaneous switching noise (SSN) that can propagate across the PCB through the cavities made by power planes [17–22]. Moreover, discontinuities along the high-speed interconnects, such as vias and imbalances in differential traces are also a source of noise [23–28].

The EBG structure is a simple and efficient way to minimize this noise. It is implemented in the same technology as used for manufacturing multilayer PCBs, thus without the need of extra components and expensive tools. EBG structures are effective in the GHz range where the lumped capacitors become useless due to their inherited parasitic inductance. Often, mixed-signal systems require isolation of the analog circuitry from the digital section in order to decouple the current return paths. EBGs turn to be attractive noise reduction solutions also in mixed-signal systems [29–31].

The EBG technology attracted attention of many research groups around the world. Its development led to introduction of various types of EBGs, mainly identifiable as the mushroom [13, 15, 32–35] and the planar types [16, 36]. Generally speaking, they consist of specifically designed metal planes with characteristic geometries suitably shaped to form a high impedance surface (HIS) [1]. Widespread utilization as well as optimization of planar EBGs resulted in making this technology flexible and easy to implement. In particular, simple design procedures were developed for effectively sizing the EBG cavity [37, 38], placing it at any level of a multilayer stack-up [39], and minimizing its impact on the IR-Drop of the power distribution network as well as on the signal quality of interconnects referenced to the EBG patterned plane [10, 40–42].

A planar EBG structure, placed within a typical multilayer PCB substrate, affects the propagation of the return current for interconnects being referenced to the patterned plane. Therefore, the impact on the signal integrity (SI) of digital signals has been considered, measured, and predicted [43–46]. Since a close electromagnetic interaction between the signal transmission along this type of interconnects and the resonant behavior of an EBG cavity was found, the coupling mechanisms have been deeply investigated to minimize the unintentional signal degradation. On the other hand, the capability of energy coupling between the signal interconnects and the planar EBGs has been found valuable for realization of efficient common mode filters [27, 47–49].

2 EBGs as Common Mode Filters

In the design of modern link paths for low voltage high-speed differential digital signals, one of the technical challenges is the containment of their common mode (CM) harmonic components [50, 51]. These components have a twofold negative effects: (a) a loss of signal energy due to the differential-to-common mode conversion and, consequently, an implicit attenuation of the intentional differential signal, and (b) EMI radiation when leaving the board assembly through connectors and cables. The origin of these components is always related to certain imbalance (geometrical and/or electrical) of the entire signal path, from the driver to the receiver [27, 52].

In a real-world design, completely removing the asymmetries is impractical or impossible; thus, a suitable solution to reduce the CM harmonics is to filter out the CM portion of the signal. This filtering operation is usually achieved using discrete components, which have some disadvantages: they take up space on the board, generate an additional cost, and are often lead to undesirable attenuation of the intentional differential signal.

An approach similar to the EBG layout technique, based on the periodic interrupted ground plane structure, has been introduced in [53] for the design of a common mode suppression filter. The regular planar EBG has been investigated in [54], where the effects of the patterned plane on both the common mode and the differential mode signal propagation along a differential microstrip line were studied. These principles are applied in [27, 47, 55] where a preliminary filter topology has been developed based on a simple cavity resonator. Later, the proper EBG type of a cavity was introduced for minimizing the layout area required by the filter for a given frequency [56].

A general structure of an EBG CM filter can be explained using the geometry shown in Fig. 1. The relevant geometry parameters are represented by the patch width (a), the gap between the patches (g), and the width of the interconnections between them (w), named "bridges." The filtering effect is achieved due to the resonant behavior of the cavity made by each single EBG cavity and the reference solid plane underneath. In practical applications of a real PCB layout, no vias should be placed within the patch area and no connection should be made between the patches and the reference plane.

The gaps between the patterned plane that are along the signal current return path allow energy coupling between the microstrip/EBG pair and the cavity made of the EBG and the solid plane. The return current goes back to the source flowing mainly under the microstrip. The current, always choosing the path of least impedance, in the case of a discontinuity—such as the gap along its path—follows three different paths. One is through the bridge (at LF due to the highly inductive nature of this part), another is through the patch-to-patch capacitance, and the last one is through the solid plane underneath the EBG patterned plane, as shown in Fig. 2.

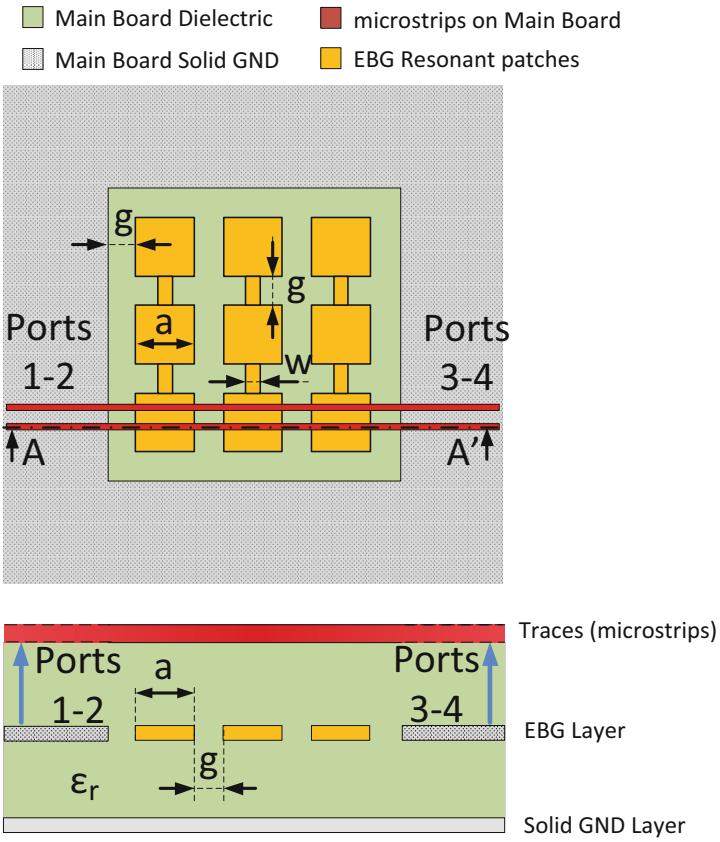

Fig. 1 Basic geometry of an EBG CM filter

The CM filter geometry needs to be appropriately sized to achieve an EBG cavity resonating at the frequency of the harmonic components that should be filtered out. Typically, for EMC purposes, these would be the fundamental and first few harmonics of the intentional differential signal. In [37], the fundamental physics of an EBG cavity is investigated, and a simple design procedure is developed in [38] to design the EBG patches and bridges according to the frequency of the CM strongest harmonic to be filtered out. Moreover, the initial procedure, based on the inductance calculation of bridges and patches as well as evaluation of the EBG equivalent inductance to its solid plane counterpart, is refined as detailed in [57], where the optimal relationships among the design variables are found, depending on the number of patches of the EBG cavity.

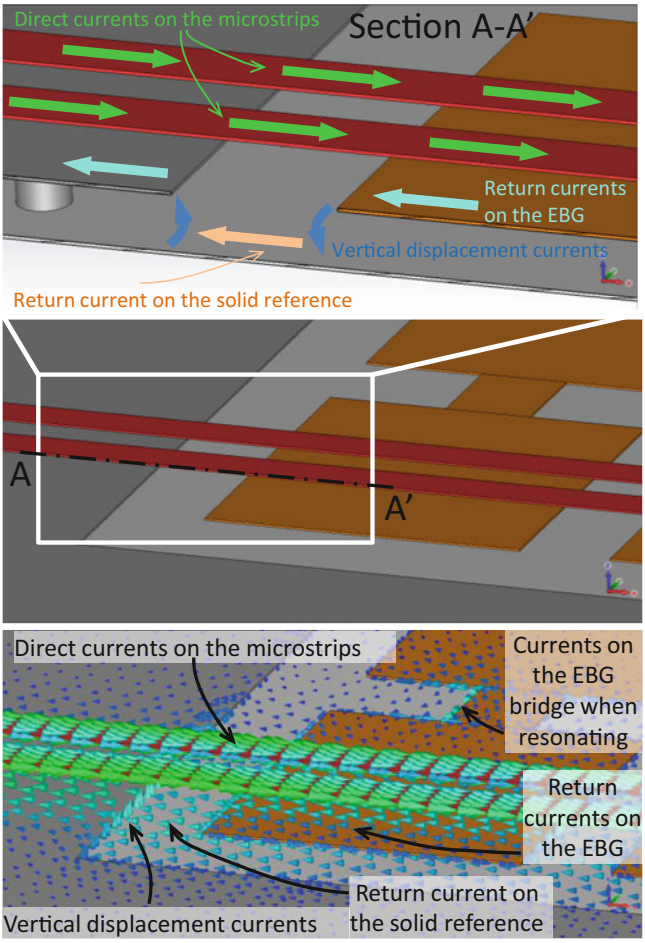

Fig. 2 Identification of the signal and return current path at the gap/bridge location

2.1 On-Board EBG-Based CM Filters

The simplest EBG-based CM filter is laid out on the PCB outermost stack-up layer (the so-called top and bottom layers). It is applied to differential microstrips as shown in Fig. 3. The figure reports the actual layout of a manufactured board which was employed to investigate the crosstalk among the adjacent differential pairs routed on the same EBG filter [58]. However, the embedded CM filters have been shown to be effective also for differential striplines [59], in which case the filter is allocated deep in the stack-up, as shown in Fig. 4. The stripline filter consists of two patterned layers above and below the differential traces, since the return current flows on both the V20 and V22 planes as in Fig. 4b. As an example, the

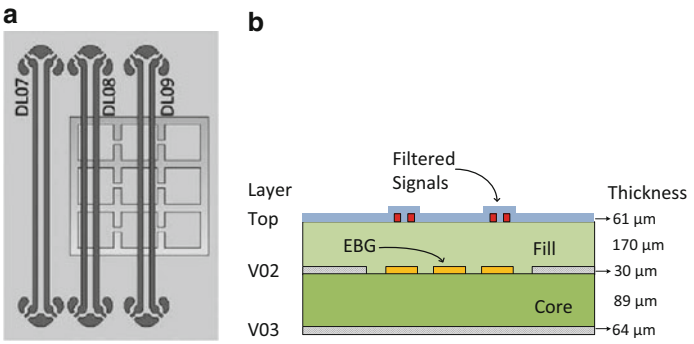

Fig. 3 Design of the microstrip experiments for the crosstalk investigation. (**a**) Top view. (**b**) Cross-section

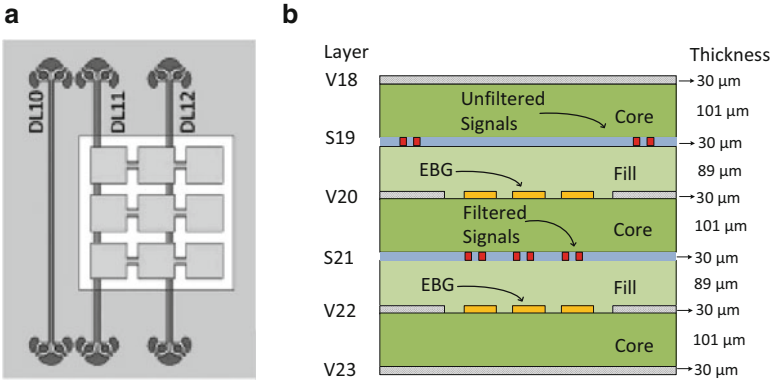

Fig. 4 Design of the stripline experiments for the crosstalk investigation. (**a**) Top view. (**b**) Cross-section

measurement results for the geometries DL08 in Fig. 3 and for the filtered stripline pair DL11 in Fig. 4 are shown in Fig. 5. The notch is clearly seen at the desired frequency of 8 GHz for the specific requirement considered for both the microstrip as well as the stripline EBG filters.

2.2 Removable EBG-Based Common Mode Filters

A different layout strategy was adopted in [60, 61] to provide more flexibility in the filter design. As opposed to the layout described in the previous paragraph, the filter has been removed from the PCB stack-up, and it is modified to be a surface-mount component installed on the top of the PCB. However, the key

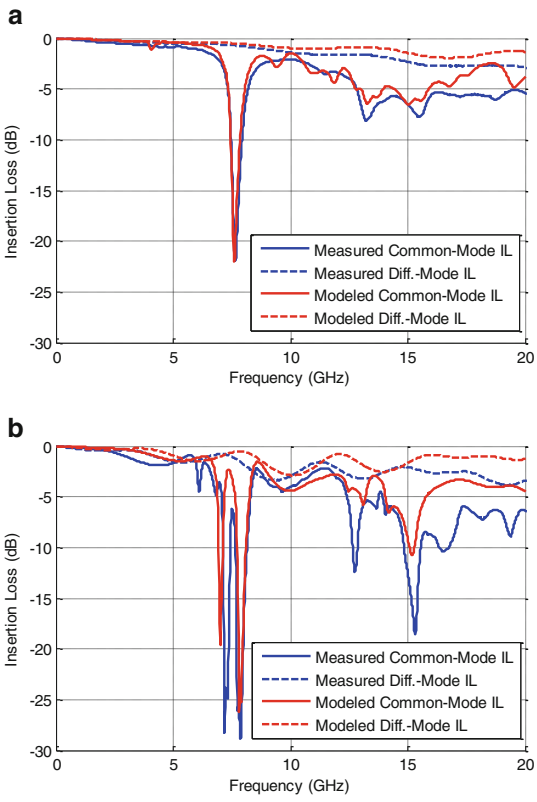

Fig. 5 CM insertion loss for the filtered (**a**) microstrip DL08, and (**b**) striplines DL11

concepts making the EBG filter attractive, such as the use of its standard multilayer laminate technology, easy design procedure, and the reduced costs, are still in place. Moreover, the electromagnetic behavior of the filter remains unchanged with the common mode return currents of the differential pair being responsible for the common mode to EBG cavity mode coupling. The drawback of having a standalone component, as mentioned before, is not a practical issue as long as the filter layout is cheap, it is designed and manufactured similarly to its on-board counterpart, and it ensures no attenuation of the intentional differential signal. The remaining disadvantage of the filter, i.e., utilization of the PCB layout area, can be minimized by employing techniques for its miniaturization; the simplest strategy is to employ a high permittivity material. Again, its larger cost compared to the standard laminates (e.g., FR-4) is not a problem due to the small size of the filter component.

A first version of the removable EBG filter was proposed in [60], where the differential pair runs on the motherboard PCB outer layer. The filter is realized in the auxiliary small PCB using the typical configuration of Fig. 6, with 3 EBG cavities, each made of three patches. The top view of the filter as well as the assembled

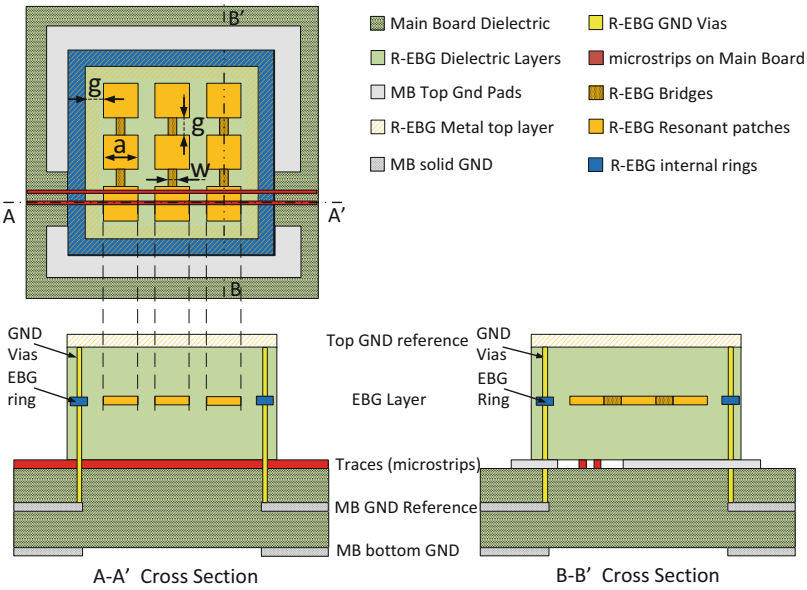

Fig. 6 (**a**) Stack-up obtained from the cut plane along the curve C1. (**b**) Path of the forward and return current at the cut plane along the curve C2. (**c**) Top view of the removable EBG filter

stack-up (the main PCB together with the removable filter) is shown in Fig. 6. The filter is attached to the PCB by means of four corner pads for the current return corresponding to pads on the PCB.

The filter can be realized by a minimum of 3-layer PCB, with the bottom one etched leaving only the four connecting pads. The second layer includes the EBG pattern and the ring; the third is the outermost solid layer for the reference ground that closes the EBG cavity. The PCB area below the EBG (layers L3 and bottom) is voided to allow the return current on L3, once it reaches the EBG area, to flow up toward the EBG through the vias and the ring. Then, the common mode return current flows back and forth between the EBG layer L1 and the top layer, as described in the previous paragraphs.

The S_{cc21} in Fig. 7 shows the predicted filter notch at 8 GHz as well as a lower one at 5.58 GHz. The latter is due to a resonant effect of the ring to ground. Moreover, the figure includes a parametric analysis to investigate the effect of the voided main PCB layers below the PCB area. The four additional models in Fig. 7a are simulated and the corresponding results are shown in Fig. 7b, c. The filter performance degradation is observed when moving the additional EBG reference closer to the filter.

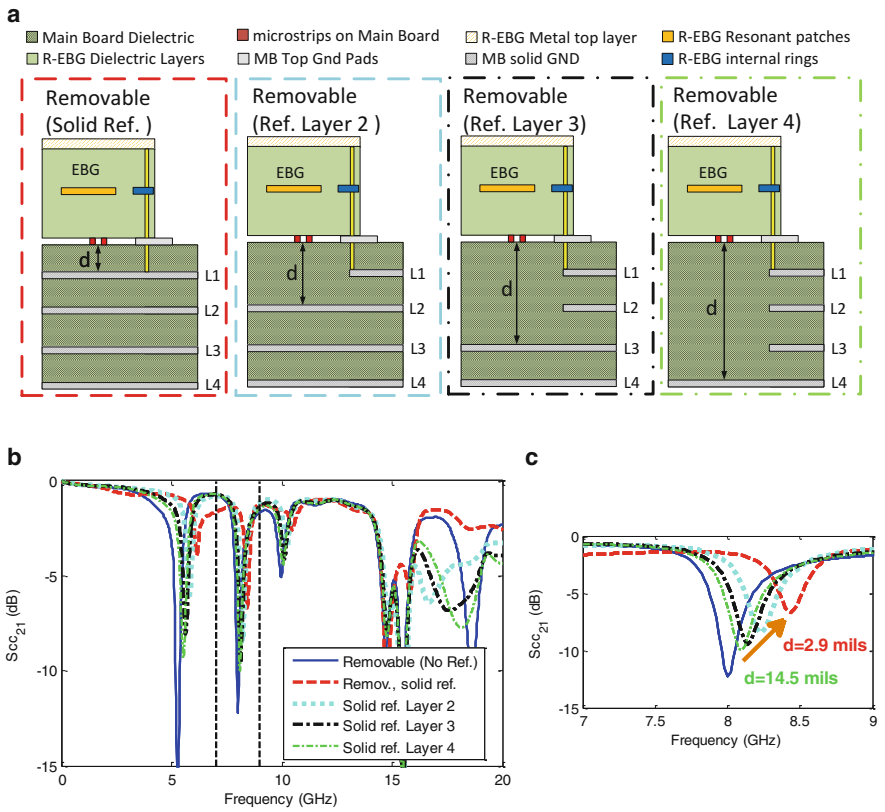

Fig. 7 Variation of the trace-to-solid reference distance. (**a**) Simulation model, (**b**) common mode insertion loss, and (**c**) zoom at the filtering notch between the two *dashed lines* in (**b**) at 7 and 9 GHz with *d* as the trace to reference distance

3 Miniaturized EBG-Based CM Filters

Maintaining small size is an important factor when including an EBG filter in the PCB layout. The present filter topology comes from a miniaturization process described in [56] where the patterned EBG cavity behaves as a resonator having smaller dimension with respect to its solid plane counterpart. Further area reduction can be achieved by manipulating the material properties of the filter. More specifically, increasing dielectric permittivity leads to smaller EBG cavity size at the same required filtering frequency. The main drawback is that materials with higher dielectric permittivity are more expensive, thus the basic design of the on-board EBG filter would require modification of the laminate material for the overall PCB. Although the present PCB technology allows to mix different dielectric layers

presented in a single stack-up (i.e., low-loss expensive materials for laying out high frequency RF or high-data-rate-line signals only on a few dielectric layers), the expensive material used for the filter dielectrics should still be employed in the overall PCB area.

This difficulty can be alleviated by utilization of the removable filter topology described in Section 2.2, thus limiting the use of high permittivity materials only for the removable filter without changing the material of the main PCB.

Two alternative designs are described in the following sub-sections and the proposed models are subsequently subjected to the optimization process (cf. Sections 4 and 5).

3.1 On-Board LTCC EBG-Based CM Filter (Model I)

The first design consists of the simplest layout as in Fig. 1 with the use of the high permittivity material on the overall board. Although this model is not quite practical due to relatively large amount of expensive laminate utilized in it, it is considered here as a preliminary illustration example of the optimization procedure.

The material employed is a Low Temperature Co-fired Ceramic (LTCC) typical for aerospace applications. As expected, the stack-up parameters changed with respect to the standard PCB technology employed for the previous filter topologies. In particular, the relative dielectric permittivity of the LTCC is 7.8 with tangent loss of 0.0045. The metal layers are made by a $2.1 \cdot 10^7$ S/m gold allowing 8 μm layer thickness, whereas the employed dielectric has a standard thickness of 137 μm.

The preliminary non-optimized model is shown in Fig. 8 based on the stack-up in Fig. 1. Since the filter is based on an EBG cavity embedded within a larger layout, a key aspect would be to reduce the electromagnetic interference induced across the surrounding signals and vias [62]. Therefore the stitching vias are laid out to minimize the EBG radiation within the same multilayer circuit. The via diameter is set to 130 μm with a distance $s = 400$ μm from the EBG area and 600 μm via-to-via distance.

During the optimization process the variation of the patch and bridge sizes would lead to the overall EBG area resize; the placement of the stitching vias in the simulation model is defined to allow the automatic via number variation according to the overall EBG area.

The EBG parameters involved in the optimization process are the patch width a, the bridge length g, and the bridge width w. These parameters will be varied to achieve the optimization targets as described in the next paragraph.

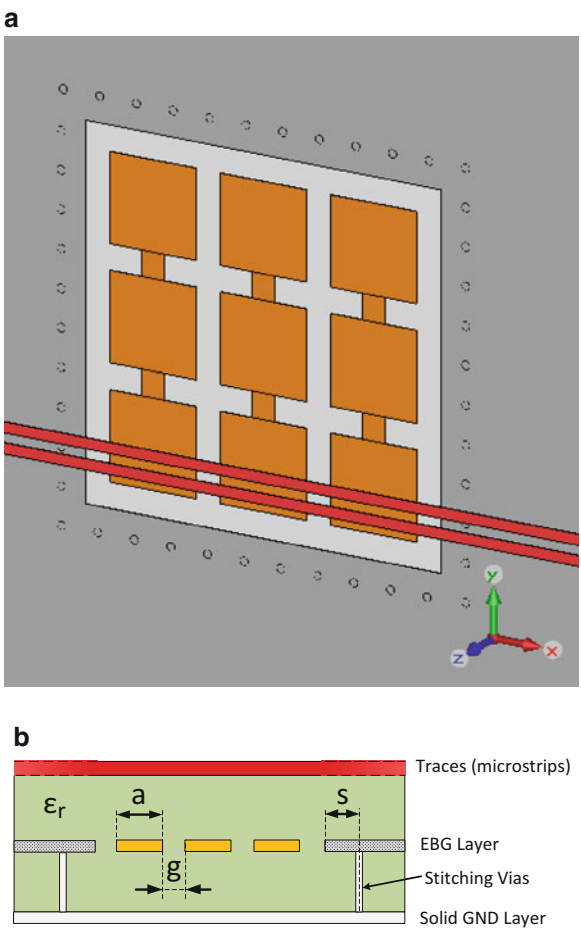

Fig. 8 (**a**) Layout of the Model I, (**b**) cross-section

3.2 Removable LTCC EBG-Based CM Filter (Model II)

The second model represents an advancement with respect to the removable EBG filter introduced in Section 2.2. Its architecture is developed to avoid the necessity of using the main board void planes below the filter footprint. To this end, the differential interconnects are moved to the removable component instead of being laid out on the main board. More specifically, the main board microstrips go up inside the removable components through the pads on the main board connected to the pads and vias on the filter substrate, as sketched in Fig. 9. The blue area surrounding the EBG layers acts as the shielding fence to minimize the radiation at the EBG filter resonance; the top solid layer of the filter is designed for the same EMI reduction purpose, thus providing a complete shielding. The finalized layout of the main board external layer as well as of the filter bottom layer is shown in Fig. 10

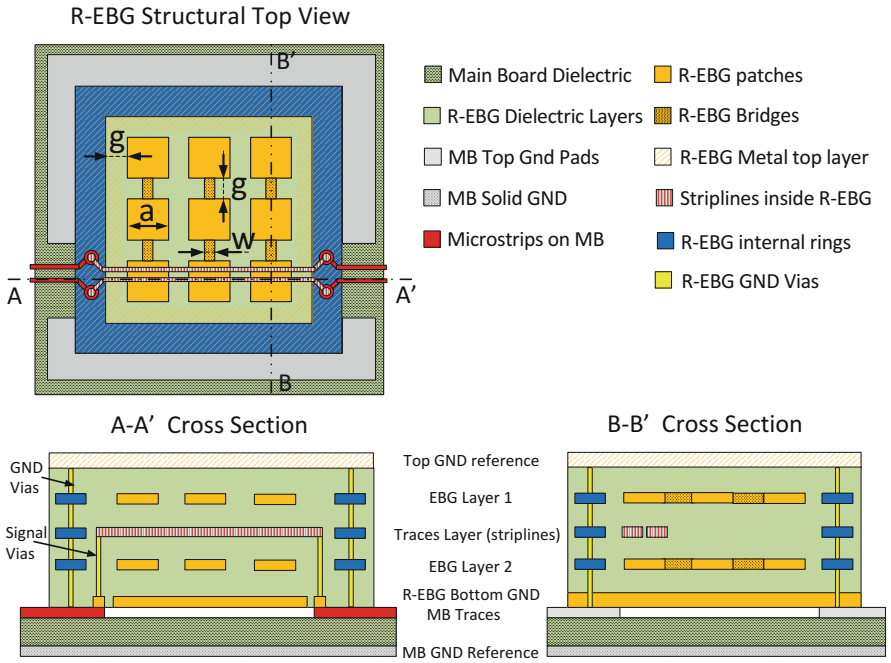

Fig. 9 Details of Model II: top view and cross-sections

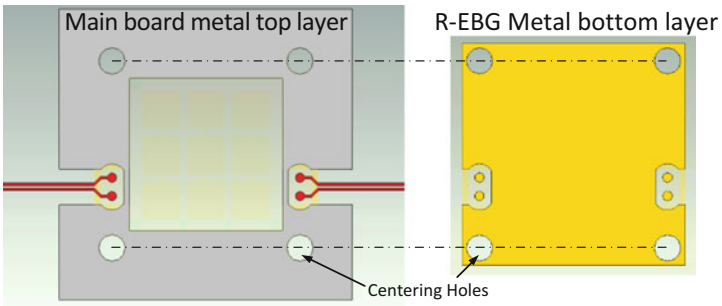

Fig. 10 Details of the external layers to be assembled on the main board and on the removable filter

to highlight the contact points between the main board and the removable filter as well as the four holes necessary for the correct board-to-filter alignment during the assembly process.

Although the layout of this proposed filter topology appears to be much more complex than the filter in Section 3.1, the EBG resonant principles remain the same, thus the variables to be varied to optimize the filter response are still those defined in Section 3.1, the patch width a, the bridge length g, and the bridge width w.

4 Filter Optimization

In this section, we describe the optimization methodology developed and utilized to improve the electrical performance parameters of the EBG filters considered in the previous paragraph. It should be emphasized that the problem at hand is challenging from the numerical point of view because of highly nonlinear responses of the EBG structures that are also very sensitive to geometry parameters. Furthermore, the computational cost of electromagnetic simulations, carried out by using *CST Studio Suite 2015* [63] of the EBG filters, is high so that one of our concerns is to limit the number of simulations as much as possible. On the other hand, the dimensionality of the design space is rather low (typically up to four parameters) which allows us to utilize auxiliary data-driven surrogate models to speed up the design optimization process.

4.1 Problem Formulation

The problem at hand is to adjust the geometry parameters of the EBG filter so that a notch is allocated at a specific design (or center) frequency f_0 (here, 8 GHz) and optimized either to (1) minimize $|S_{21}|$ in a frequency band $f_0 - df \le f \le f_0 + df$ (here, $df = 0.1$ GHz), or to (2) increase the bandwidth for which $|S_{21}| \le -10$ dB.

In more rigorous terms, the problem can be formulated as follows:

$$\boldsymbol{x}^* = \arg\min_{\boldsymbol{x}} U\left(\boldsymbol{R}\left(\boldsymbol{x}\right)\right) \tag{1}$$

where $\boldsymbol{R}$ denotes a response vector of the EM simulation model of the EBG filter (here, S-parameters versus frequency), $\boldsymbol{x}$ is a vector of designable geometry parameters, and U is the objective function. The objective function is defined either as

$$U\left(\boldsymbol{R}\left(\boldsymbol{x}\right)\right) = U\left(\left|S_{21}\left(\boldsymbol{x};f\right)\right|\right) = \max\left\{\left|S_{21}\left(\boldsymbol{x};f\right)\right|_{f_0-df\le f\le f_0+df}\right\} \tag{2}$$

for case (1) or

$$\begin{aligned} U\left(\boldsymbol{R}\left(\boldsymbol{x}\right)\right) = U\left(\left|S_{21}\left(\boldsymbol{x};f\right)\right|\right) &= \arg\min_{f}\left\{\left|S_{21}\left(\boldsymbol{x};f\right)\right| \le -10\ \text{dB}\right\} \\ &- \arg\max_{f}\left\{\ \left|S_{21}\left(\boldsymbol{x};f\right)\right| \le -10\ \text{dB}\right\} \end{aligned} \tag{3}$$

for case (2).

The geometry parameters are a = patch width, g = bridge length, and w = bridge width forming the geometry parameters vector $\boldsymbol{x} = [a\ g\ w]^T$.

The problem (1) is constrained as follows:

- Lower and upper bounds for geometry parameters $\boldsymbol{l} \le \boldsymbol{x} \le \boldsymbol{u}$, and
- Linear inequality constraints $c_k(\boldsymbol{x}) \le 0$, $k = 1, \ldots, K$.

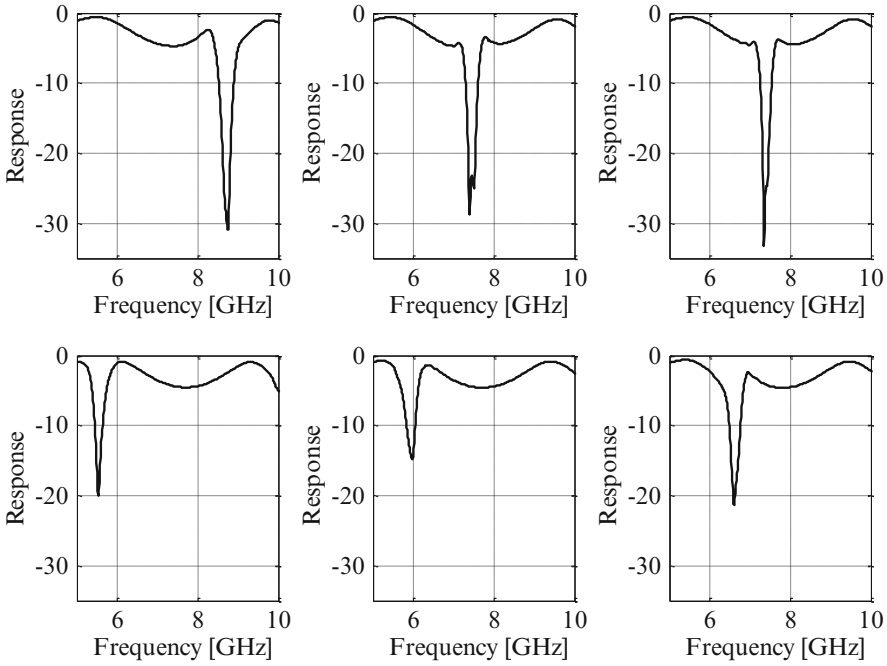

Fig. 11 Responses of the EBG filter at various parameter setups. One can observe that the responses are highly nonlinear (as a function of frequency) and very sensitive to the adjustable parameters of the problem

The constraints are introduced to make the structure physically consistent and able to fulfill the limits of the building technology.

It should be emphasized that the optimization problem is challenging because of sharp narrow responses in the notch region. The typical responses of the filter at various design parameter setup, indicating the difficulty of the problem at hand, are shown in Fig. 11. It can be observed that depending on the initial design, local optimization may fail to find a satisfactory design. Thus, local optimization has to be preceded by a screening stage at which the notch is approximately allocated around f_0 as required.

4.2 Optimization Algorithm

The initial screening mentioned in Section 4.1 cannot be executed through conventional global optimization using, e.g., population-based meta-heuristics due to excessive computational cost associated with such procedures. On the other hand, we are not interested in a precise control of the entire filter response but just in handling its two critical features, i.e., the center frequency and the depth

of the notch. It turns out that despite highly nonlinear dependence of the *S*-parameter responses of the filter on frequency, the aforementioned features of the notch (both its center frequency and depth), change much more linearly with the design variables. Additionally, the number of geometry parameters is small so that is it possible to construct and exploit a data-driven model of the notch features. In this work, Kriging interpolation [64] is utilized for model construction. More specifically, the following procedure is implemented and employed to find a reasonable starting point for further local optimization:

(1) Sample the design space at N locations $\boldsymbol{x}_B^{(k)}$, $k = 1, \ldots, N$;
(2) Evaluate the EM model $\boldsymbol{R}$ at all points obtained in Step 1;
(3) Extract center frequencies $f_B^{(k)}$ and notch depths $L_B^{(k)}$ for all the points;
(4) Construct a Kriging interpolation models $s_f(\boldsymbol{x})$ and $s_L(\boldsymbol{x})$ of the center frequencies and depths as a function of design variables;
(5) Optimize the Kriging models in order to allocate the notch at the required frequency $f_0 = 8$ GHz and increase its depth L.

The objective function used in Step 5 is as follows: $U_L(\boldsymbol{x}) = s_L(\boldsymbol{x}) + \beta \cdot \left[\left(s_f(\boldsymbol{x}) - f_0\right)/f_0\right]^2$. Such a formulation allows for increasing the notch depth while centering it at the required operating frequency.

For illustration purposes, Fig. 12 shows the landscapes of the Kriging model (notch depth and its center frequency) for three various values of the patch width a of 1.5, 1.71, and 2.0 mm for the EBG filter of Fig. 8.

Having the notch allocated around the required frequency by optimizing the Kriging interpolation models, local optimization is executed. Here, a pattern search algorithm [65] is utilized because of low-dimensionality of the search space. In case of a larger number of parameters more efficient methods would have to be used.

5 Numerical Results

In this section, we provide optimization results of the two EBG filters considered in this chapter. Optimization was executed using the methodology described in Section 4.

5.1 On-Board LTCC EBG-Based CM Filter (Model I)

In case of Model I, only the lower $\boldsymbol{l}$ and upper $\boldsymbol{u}$ bounds for design variables were set as follows: $\boldsymbol{l} = [0.836\ 0.15\ 0.15]^T$ mm and $\boldsymbol{u} = [2.0\ 1.0\ 1.0]^T$ mm. There was no need to execute the initial screening because the notch was allocated sufficiently close to the center frequency of 8 GHz at the initial design $\boldsymbol{x}^{init} = [1.4000\ 0.4036\ 0.3750\ 0.4030]^T$. The local search was only run for case (2) of Section 4.1 (bandwidth maximization) and resulted in the final design $\boldsymbol{x}^* = [1.3444\ 0.0.3969\ 0.02789]^T$.

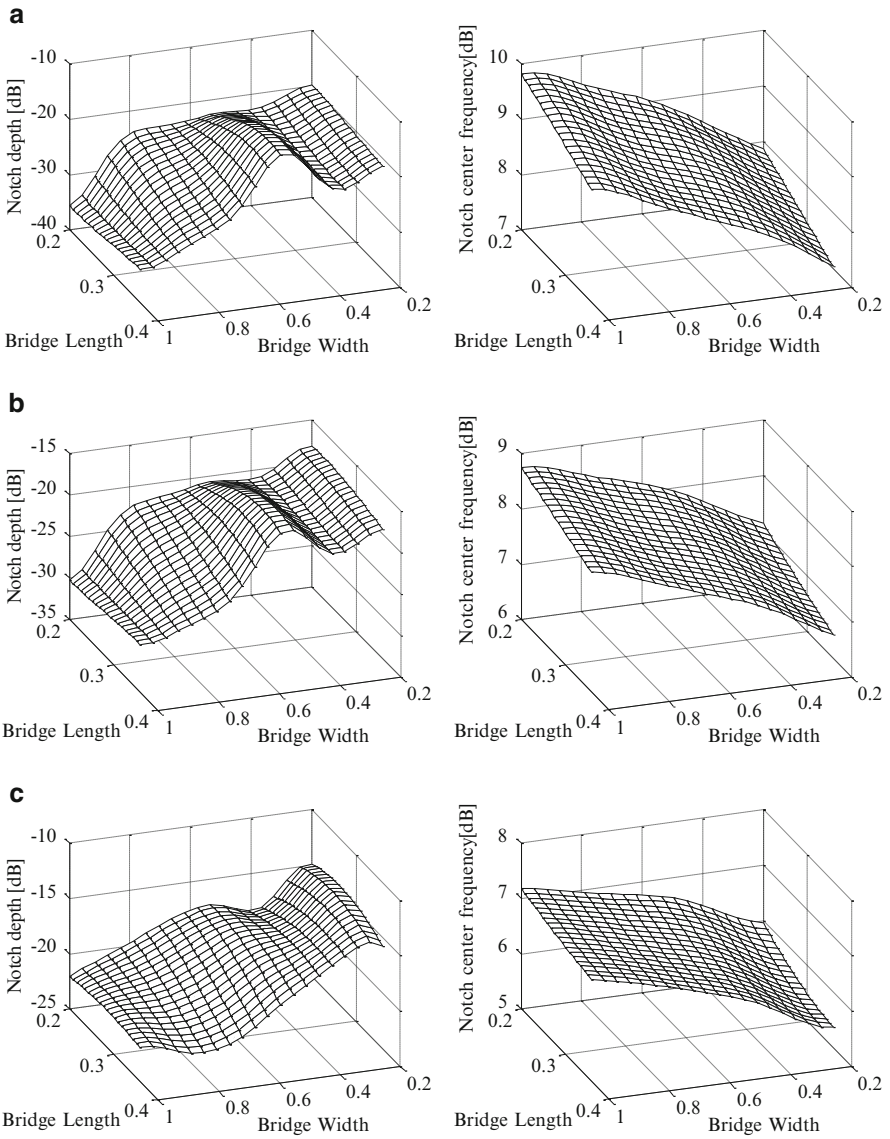

Fig. 12 Two-dimensional cuts of the Kriging interpolation models $s_f(\mathrm{x})$ and $s_L(\mathrm{x})$ for the EBG filter of Fig. 8, corresponding to patch width $a = 1.5$ (**a**), 1.71 (**b**), and 2.0 (**c**)

Fig. 13 shows the responses of the filter at the initial and at the final design. The design cost is 45 evaluations of the EM filter model. It can be observed that both the notch depth and the bandwidth were greatly improved compared to the initial design. Also, the bandwidth at the final design is centered at the frequency $f_0 = 8$ GHz as required.

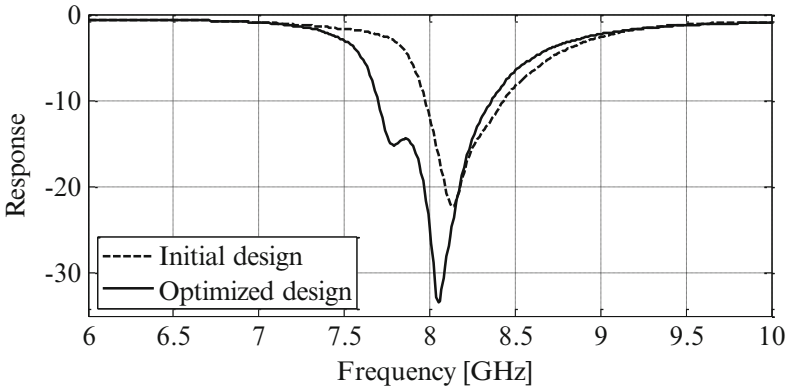

Fig. 13 EBG filter (Model I) responses at the initial and the optimized designs

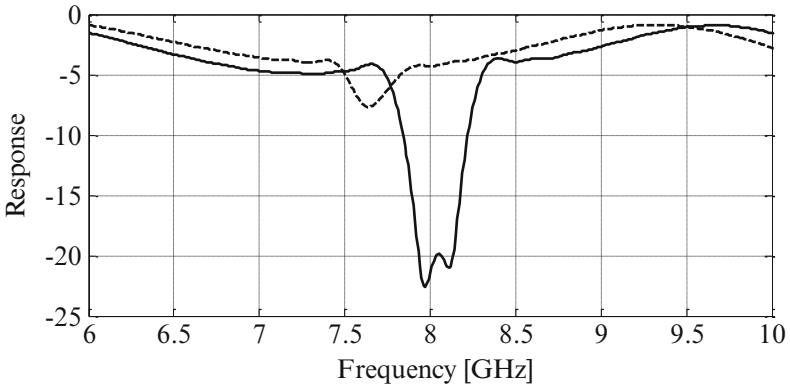

Fig. 14 Responses of the EBG filter (Model II) at the initial design *dashed line* and at the design obtained at the first stage of the optimization process (screening) *solid line*

5.2 Removable LTCC EBG-Based CM Filter (Model II)

In this case of Model II, the following lower and upper bounds for design variables were set: $\boldsymbol{l} = [0.836\ 0.15\ 0.15]^T$ mm and $\boldsymbol{u} = [2.0\ 1.0\ 1.0]^T$ mm. Additionally, the following two inequality constraints were defined: $2*w + 2*g \leq 6.385$ and $w \leq a$. The result obtained in the screening stage is $\boldsymbol{x}^{init} = [1.5000\ 0.2733\ 0.3489]^T$. The EM-simulated response is shown in Fig. 14. The design is already very good both in terms of the notch frequency and depth. Dashed line shows the initial design $[2.500\ 0.400\ 0.175]^T$, which is very poor, especially in terms of the notch depth. The cost of the screening stage was 48 evaluations of the EM filter model required to set up the Kriging interpolation model.

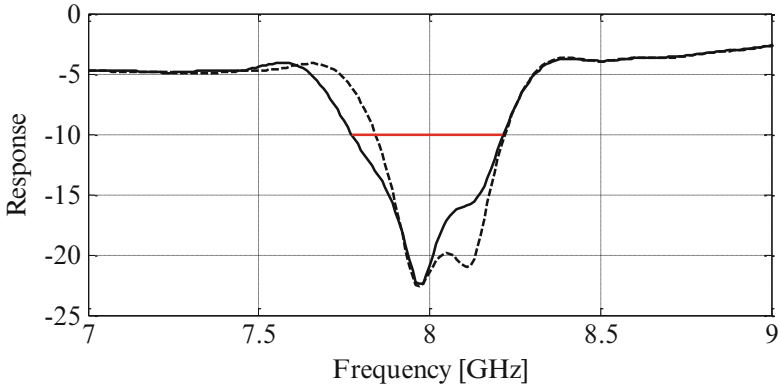

Fig. 15 Local optimization of the EBG filter (Model II) for case (1) (bandwidth enhancement): *dashed line* initial design from screening, *solid line* final design

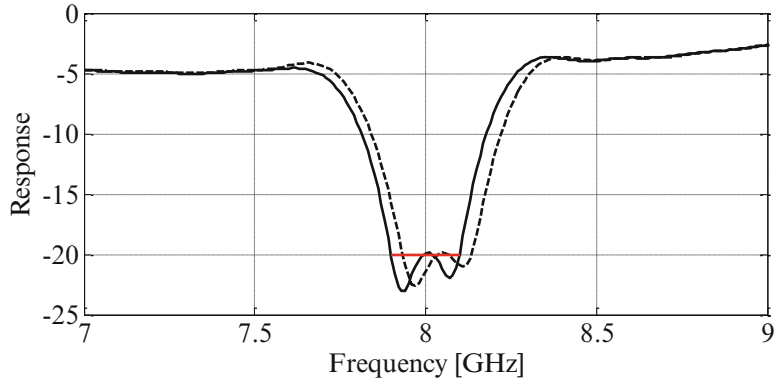

Fig. 16 Local optimization of the EBG filter (Model II) for case (2) (notch depth): *dashed line* initial design from screening, *solid line* final design

Figures 15 and 16 show the filter responses at the two designs obtained by local optimization starting from $\boldsymbol{x}^{init}$, the first one for case (1) (bandwidth enhancement) and case (2) (notch depth enhancement): $\boldsymbol{x}^{*1} = [1.5000\ 0.2733\ 03558]^T$ and $\boldsymbol{x}^{*2} = [1.5000\ 0.2733\ 03451]^T$. The -10 dB bandwidth obtained in the first case is 442 MHz and it is wider than for the second design (365 MHz). On the other hand, the second design exhibits notch depth of -20 dB and better for the frequency range of 7.9–8.1 GHz, which is not the case for the first design. The cost of the local optimization was only 15 and 19 EM model evaluations for case (1) and case (2), respectively, which is because the final designs were close to the one obtained at the screening stage.

6 Conclusions

In the chapter, an efficient numerical procedure for EM-simulation-driven design optimization of EBG-based filters has been presented. The design objectives are to obtain the band-notch at a specified center frequency and increase the notch bandwidth and depth, and, consequently, the bandwidth of the common mode insertion loss. The optimization algorithm is applied to two different topologies, initially designed employing a previously published analytical procedure. The first case is based on a typical PCB configuration where the filter is laid out within the PCB stack-up. The second filter structure consists of a more complex topology with the filter modified with respect to the typical on-board case. At the conceptual level, the goal is to develop a miniaturized standalone component (still designed with the typical PCB/package planar layout) to be removed and substituted if necessary once the electronics of the system changes, i.e. when the data rate and thus the common mode harmonic components or simply the design requirements are modified.

The proposed optimization algorithm can be applied at the design closure stage to fine-tune the geometry parameters of the EBG filters. It allows for automation and reduction of the computational cost of the simulation-driven design, previously realized using inefficient and error-prone hands-on procedures involving parameter sweeps. The future work will include further developments of the algorithmic frameworks for EBG filter optimization as well as its application to various practical design cases.

References

1. Sievenpiper, D., Zhang, L., Broas, R.F.J., Alexopulos, N.G., Yablonovitch, E.: High-impedance electromagnetic surfaces with a forbidden frequency band. IEEE Trans. Microw. Theory Tech. **47**(11), 2059–2073 (1999)
2. Tan, M.N.M., Ali, M.T., Subahir, S., Rahman, T.A., Rahim, S.K.A.: Backlobe reduction using mushroom-like EBG structure. In: Proceedings of IEEE Symposium on Wireless Technology and Applications (ISWTA), pp. 206–209, 23–26 September 2012
3. Chen, X., Su, Z.J., Li, L., Liang, C.H.: Radiation pattern improvement in closely-packed array antenna by using mushroom-like EBG structure. In: Radar Conference 2013, IET International, pp. 1–3, 14–16 April 2013
4. Neo, C., Lee, Y.H.: Patch antenna enhancement using a mushroom-like EBG structures. In: Antennas and Propagation Society International Symposium (APSURSI), 2013 IEEE, pp. 614–615, 7–13 July 2013
5. Coulombe, M., Koodiani, S.F., Caloz, C.: Compact elongated mushroom (EM)-EBG structure for enhancement of patch antenna array performances. IEEE Trans. Antennas Propag. **58**(4), 1076–1086 (2010)
6. Azad, M.Z., Ali, M.: Novel wideband directional dipole antenna on a mushroom like EBG structure. IEEE Trans. Antennas Propag. **56**(5), 1242–1250 (2008)
7. Qin, J., Ramahi, O.M., Granatstein, V.: Novel planar electromagnetic bandgap structures for wideband noise suppression and EMI reduction in high speed circuits. IEEE Trans. Electromagn. Compat. **49**(3), 661–669 (2007)

8. Wu, T.L., Wang, C.C., Lin, Y.H., Wang, T.K., Chang, G.: A novel power plane with super-wideband elimination of ground bounce noise on high speed circuits. IEEE Microw. Wireless Compon. Lett. **15**(3), 174–176 (2005)
9. Shapharnia, S., Ramahi, O.M.: Electromagnetic interference (EMI) reduction from printed circuit boards (PCB) using electromagnetic bandgap structures. IEEE Trans. Electromagn. Compat. **46**(4), 580–587 (2004)
10. de Paulis, F., Nisanci, M.N., Orlandi, A.: Practical EBG application to multilayer PCB: Impact on power integrity. IEEE Electromagn. Compat. Mag. **1**(3), 60–65 (2012)
11. Wu, T.L., Lin, Y.H., Wang, T.K., Wang, C.C., Chen, S.T.: Electromagnetic bandgap power/ground planes for wideband suppression of ground bounce noise and radiated emission in highspeed circuits. IEEE Trans. Microw. Theory Tech. **53**(9), 2935–2942 (2005)
12. Kamgaing, T., Ramahi, O.M.: A novel power plane with integrated simultaneous switching noise mitigation capability using high impedance surface. IEEE Microw. Wireless Compon. Lett. **13**(1), 21–23 (2003)
13. Abhari, R., Eleftheriades, G.V.: Metallo-dielectric electromagnetic bandgap structures for suppression and isolation of the parallel-plate noise in high-speed circuits. IEEE Trans. Microw. Theory Tech. **51**(6), 1629–1639 (2003)
14. Tavallaee, M. Iacobacci, Abhari, R.: A new approach to the design of power distribution networks containing electromagnetic bandgap structures. Electr. Perform. Elect. Packag. (EPEP) conference, 43–46 (2006)
15. Kamgaing, T., Ramahi, O.M.: Design and modeling of high impedance electromagnetic surfaces for switching noise suppression in power planes. IEEE Trans. Electromagn. Compat. **47**(3), 479–489 (2005)
16. Kim, K.H., Shutt-Ainé, J.E.: Analysis and modeling of hybrid planar-type electromagnetic-bandgap structures and feasibility study on power distribution network applications. IEEE Trans. Microw. Theory Tech. **56**(1), 178–186 (2008)
17. Swaminathan, M., Engin, A.E.: Power Integrity Modeling and Design for Semiconductors and Systems. Prentice Hall, Boston, USA (2008)
18. Lei, G.-T., Techentin, R.W., Gilbert, B.K.: High frequency characterization of power/ground-plane structures. IEEE Trans. Microw. Theory Tech. **47**, 562–569 (1999)
19. Berghe, S.V., Olyslager, F., de Zutter, D., Moerloose, J.D., Temmerman, W.: Study of the ground bounce caused by power plane resonances. IEEE Trans. Electromagn. Compat. **40**(2), 111–119 (1998)
20. Cui, W., Fan, J., Ren, Y., Shi, H., Drewniak, J.L., DuBroff, R.E.: DC power-bus noise isolation with power-plane segmentation. IEEE Trans. Electromagn. Compat. **45**(2), 436–443 (2003)
21. Na, N., Jinseong, J., Chun, S., Swaminathan, M., Srinivasan, J.: Modeling and transient simulation of planes in electronic packages. IEEE Trans. Adv. Packag. **23**(3), 340–352 (2000)
22. Xu, M., Hubing, T.H., Chen, J., Van Doren, T.P., Drewniak, J.L., DuBroff, R.E.: Power-bus decoupling with embedded capacitance in printed circuit board design. IEEE Trans. Electromagn. Compat. **45**(1), 22–30 (2003)
23. Huang, W.-T., Lu, C.-H., Lin, D.-B.: The optimal number and location of grounded vias to reduce crosstalk. Prog. Electromagn. Res. **95**, 241–266 (2009)
24. Wu, B., Tsang, L.: Full-wave modeling of multiple vias using differential signaling and shared antipad in multilayered high speed vertical interconnects. Prog. Electromagn. Res. **97**, 129–139 (2009)
25. de Paulis, F., Zhang, Y.-J., Fan, J.: Signal/power integrity analysis for multilayer printed circuit boards using cascaded S-parameters. IEEE Trans. Electromagn. Compat. **52**(4), 1008–1018 (2010)
26. Wu, B., Tsang, L.: Full-wave modeling of multiple vias using differential signaling and shared antipad in multilayered high speed vertical interconnects. Prog. Electromagn. Res. **97**, 129–139 (2009)
27. de Paulis, F., Archambeault, B., Connor, S., Orlandi, A.: Electromagnetic band gap structure for common mode filtering of high speed differential signals. In: Proceedings of IEC DesignCon 2011, Santa Clara, USA, 31 January–3 February 2011

28. Ricchiuti, V., de Paulis, F., Orlandi, A.: An equivalent circuit model for the identification of the stub resonance due to differential vias on PCB. In: Proceedings of IEEE Workshop on Signal Propagation on Interconnects 2009, SPI '09, Strasbourg, France, 12–15 May 2009
29. Choi, J., Govind, V., Mandrekar, R., Janagama, S., Swaminathan, M.: Noise reduction and design methodology for the mixed-signal systems with alternating impedance electromagnetic bandgap (Al-EBG) structure. In: International Microwave Symposium Digest, Long Beach, CA, pp. 645–651, June 2005
30. Kim, T.H., Chung, D., Engin, E., Yun, W., Toyota, Y., Swaminathan, M.: A novel synthesis method for designing electromagnetic bandgap (EBG) structures in packaged mixed signal systems. In: Proceedings of 56th Electronic Components and Technology Conference, pp. 1645–1651, 2006
31. Rajo-Iglesias, E., Caiazzo, M., Inclán-Sánchez, L., Kildal, P-.S.: Comparison of bandgaps of mushroom-type EBG surface and corrugated and strip-type soft surfaces. IET Microw. Antennas Propag. **1**(1), 184–189 (2007)
32. Liang, L., Liang, C.H., Chen, L., Chen, X.: A novel broadband EBG using cascaded mushroom-like structure. Microw. Opt. Technol. Lett. **50**, 2167–2170 (2008)
33. Kamgaing, T., Ramahi, O.M.: Multiband electromagnetic-bandgap structures for applications in small form-factor multichip module packages. IEEE Trans. Microw. Theory Tech. **56**(10), 2293–2300 (2008)
34. Wu, T.L., Fan, J., de Paulis, F., Wang, C.D., Ciccomancini, A., Orlandi, A.: Mitigation of noise coupling in multilayer high-speed PCB: State of the art modeling methodology and EBG technology. IEICE Trans. Commun. **E93-B**(7), 1678–1689 (2010)
35. Wang, C.-D., Yu, Y.-M., de Paulis, F., Scogna, A.C., Orlandi, A., Chiou, Y.-P., Wu, T.-L.: Bandwidth enhancement based on optimized via location for multiple vias EBG power/ground planes. IEEE Trans. Compon. Packag. Manuf. Technol. **2**(2), 332–341 (2012)
36. Oh, S.S., Kim, J.M., Kwon, J.H., Yook, J.G.: Enhanced power plane with photonic bandgap structures for wide band suppression of parallel plate resonances. In: IEEE International Symposium on Antennas and Propagation, vol. 2B, pp. 655–658, July 2005
37. de Paulis, F., Orlandi, A.: Accurate and efficient analysis of planar electromagnetic band-gap structures for power bus noise mitigation in the GHz band. Prog. Electromagn. Res. B **37**, 59–80 (2012)
38. Raimondo, L., de Paulis, F., Orlandi, A.: A simple and efficient design procedure for planar electromagnetic bandgap structures on printed circuit boards. IEEE Trans. Electromagn. Compat. **53**(2), 482–490 (2011)
39. de Paulis, F., Raimondo, L., Orlandi, A.: Impact of shorting vias placement on embedded planar electromagnetic bandgap structures within multilayer printed circuit boards. IEEE Trans. Microw. Theory Tech. **58**(7), 1867–1876 (2010)
40. de Paulis, F., Raimondo, L., Orlandi, A.: IR-Drop analysis and thermal assessment of planar electromagnetic band-gap structures for power integrity applications. IEEE Trans. Adv. Packag. **33**(3), 617–622 (2010)
41. Di Febo, D., Nisanci, M.H., de Paulis, F., Orlandi, A.: Impact of planar electromagnetic band-gap structures on IR-DROP and signal integrity in high speed printed circuit boards. In: Proceedings at IEEE International Symposium on EMC – EMC Europe 2012, Rome, Italy, 17–21 September 2011
42. Nisanci, M.N., de Paulis, F., Di Febo, D., Orlandi, A.: Practical EBG application to multilayer PCB: Impact on signal integrity. IEEE Electromagn. Compat. Mag. **2**(2), 82–87 (2013)
43. Scogna, A.C., Orlandi, A., Ricchiuti, V.: Signal and power integrity performances of striplines in presence of 2D EBG planes. In: Proceedings of IEEE Workshop on Signal Propagation and Interconnects, Avignon, France, May 2008
44. de Paulis, F., Orlandi, A.: Signal integrity analysis of single-ended and differential striplines in presence of EBG planar structures. IEEE Microw. Wireless Compon. Lett. **19**(9), 554–556 (2009)

45. de Paulis, F., Orlandi, A., Raimondo, L., Antonini, G.: Fundamental mechanisms of coupling between planar electromagnetic bandgap structures and interconnects in high-speed digital circuits—Part I: Microstrip lines. Presented at the Electromagnetic Compatibility Europe Workshop, Athens, Greece, 11–12 June 2009
46. de Paulis, F., Raimondo, L., Orlandi, A.: Signal integrity analysis of embedded planar EBG structures. In: Proceedings of Asia-Pacific EMC 2010, Beijing, China, 12–16 April 2010
47. de Paulis, F., Raimondo, L., Connor, S., Archambeault, B., Orlandi, A.: Design of a common mode filter by using planar electromagnetic bandgap structures. IEEE Trans. Adv. Packag. **33**(4), 994–1002, 2010
48. de Paulis, F., Raimondo, L., Connor, S., Archambeault, B., Orlandi, A.: Compact configuration for common mode filter design based on electromagnetic band-gap structures. IEEE Trans. Electromagn. Compat. **54**(3), 646–654 (2012)
49. de Paulis, F., Raimondo, L., Di Febo, D., Archambeault, B., Connor, S., Orlandi, A.: Experimental validation of common-mode filtering performances of planar electromagnetic band-gap structures. In: Proceedings of IEEE International Symposium on Electromagnetic Compatibility, Ft. Lauderdale, USA, 25–30 July 2010
50. Archambeault, B.: PCB Design for Real-World EMI Control. Kluwer Academic Publisher, Norwell, MA (2002)
51. Connor, S., Archambeault, B., Mondal, M.: The impact of common mode currents on signal integrity and EMI in high-speed differential data links. In: Proceedings of IEEE International Symposium on Electromagnetic Compatibility, pp. 1–5, 18–22 August 2008
52. Jaze, A., Archambeault, B., Connor, S.: Differential mode to common mode conversion on differential signal vias due to asymmetric GND via configurations. In: Proceedings of IEEE International Symposium on Electromagnetic Compatibility, pp. 735–740, 5–9 August 2013
53. Liu, W.T., Tsai, C.H., Han, T.W., Wu, T.L.: An embedded common-mode suppression filter for GHz differential signals using periodic defect ground plane. IEEE Microw. Wireless Compon. Lett. **18**(4), 248–250 (2008)
54. de Paulis, F., Orlandi, A., Raimondo, L., Archambeault, B., Connor, S.: Common mode filtering performances of planar EBG structures. In: Proceedings of IEEE International Symposium on Electromagnetic Compatibility, pp. 86–90, 17–21 August 2009
55. de Paulis, F., Raimondo, L., Di Febo, D., Orlandi, A.: Routing strategies for improving common mode filter performances in high speed digital differential interconnects. In: Proceedings of IEEE Workshop on Signal Propagation on Interconnects 2011, SPI '11, Naples, Italy, 8–11 May 2011
56. de Paulis, F., Archambeault, B., Nisanci, M.H., Connor, S., Orlandi, A.: Miniaturization of common mode filter based on EBG patch resonance. In: Proceedings of IEC DesignCon 2012, Santa Clara, USA, 30 January–2 February 2012
57. Nisanci, M.H., de Paulis, F., Orlandi, A., Archambeault, B., Connor, S.: Optimum geometrical parameters for the EBG-based common mode filter design. In: Proceedings at 2012 IEEE Symposium on Electromagnetic Compatibility, Pittsburgh, PA, USA, 5–10 August 2012
58. de Paulis,F., Cracraft, M., Di Febo, D., Nisanci, M.H., Connor, S., Archambeault, B., Orlandi, A.: EBG-based common-mode microstrip and stripline filters: Experimental investigation of performances and crosstalk. IEEE Trans. Electromagn. Compat. **57**(5), 996–1004 (2015)
59. de Paulis, F., Cracraft, M., Olivieri, C., Connor, S., Orlandi, A., Archambeault, B.: EBG-based common-mode stripline filters: Experimental investigation on interlayer crosstalk. IEEE Trans. Electromagn. Compat. **57**(6), 1416–1424 (2015)
60. de Paulis, F., Nisanci, M.H., Di Febo, D., Orlandi, A., Connor, S., Cracraft, M., Archambeault, B.: Standalone removable EBG-based common mode filter for high speed differential signaling. In: Proceedings of IEEE International Symposium on Electromagnetic Compatibility, Raleigh NC (USA), pp. 244–249, 3–8 August 2014

61. Varner, M.A., de Paulis, F., Orlandi, A., Connor, S., Cracraft, M., Archambeault, B., Nisanci, M.H., Di Febo, D.: Removable EBG-based common-mode filter for high-speed signaling: Experimental validation of prototype design. IEEE Trans. Electromagn. Compat. **57**(4), 672–679 (2015)
62. Kodama, C., O'Daniel, C., Cook, J., de Paulis, F., Cracraft, M., Connor, S., Orlandi, A.,. Wheeler, E: Mitigating the threat of crosstalk and unwanted radiation when using electromagnetic bandgap structures to suppress common mode signal propagation in PCB differential interconnects. In: Proceedings of IEEE International Symposium on Electromagnetic Compatibility, Dresden, pp. 622–627, 16–22 August 2015
63. Computer Simulation Technology, *CST Studio Suite 2015*, available at www.cst.com
64. Queipo, N.V., Haftka, R.T., Shyy, W., Goel, T., Vaidynathan, R., Tucker, P.K.: Surrogate-based analysis and optimization. Prog. Aerosp. Sci. **41**(1), 1–28 (2005)
65. Koziel, S.: Computationally efficient multi-fidelity multi-grid design optimization of microwave structures. Appl. Comput. Electromagn. Soc. J. **25**(7), 578–586 (2010)